Thesis for the Degree of Master of Engineering

Synthesis and Design of Organic Small Molecules for Electron-Transporting Material in Organic Optoelectronic Devices

by

Jun Tae Kim

Department of Industrial Chemistry

The Graduate School

Pukyong National University

August 2019

Synthesis and Design of Organic Small Molecules for Electron-Transporting Material in Organic Optoelectronic Devices

(유기 광전자 소자에 적용 가능한 전자 수송 물질 개발을 위한 유기 단분자 물질 합성 및 설계)

Advisor: Prof. Dong Wook Chang

by

Jun Tae Kim

A thesis submitted in partial fulfillment of the requirements
for the degree of

Master of Engineering

in Department of Industrial Chemistry, The Graduate School,
Pukyong National University

August 2019

Synthesis and Design of Organic Small Molecules for Electron-Transporting Material in Organic Optoelectronic Devices

A dissertation

by

Jun Tae Kim

Approved by:

(Youngeup Jin)

(Boram Lee)

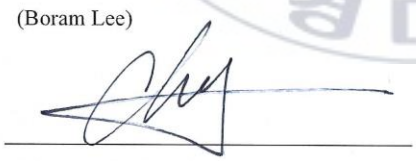

(Dongwook Chang)

August 2019

Contents

List of Figures

List of Tables

List of Schemes

유기 광전자 소자를 위한 Quinoxaline 과 Phosphine oxide 유도체를 포함하는 전자 수송 물질 합성과 응용

김 준 태

부경대학교 대학원 공업화학과

요약

유기물이 가지는 흥미로운 이점들 때문에 유기물을 이용한 유기발광소자 그리고 유기태양전지가 많은 관심을 받고 연구가 진행되어왔다. 현재 유기발광소자는 많은 연구들을 통하여 차세대 디스플레이 기술로서 상용화 되고 있으며, 유기태양전지는 고갈되는 화석연료 그리고 자원문제들로 인해 깨끗하고 지속 사용 가능한 에너지원으로 주목 받고 있다. 두 광전자소자는 일반적으로 active layer (빛을 발광하는 유기층 또는 빛을 흡수하는 유기층) 와 양극, 음극 사이에 전하를 이동시켜주는 정공전달층, 전자전달층으로 구성되어있다. 전자전달층의 interlayer 로 많이 이용되는 물질은 LiF, Ca 등이 있고, 이는 알칼리계통 금속화합물로 산소와 수분에 매우 반응성이 크고, 공기 중 안정성이 떨어진다. 그러므로 전자전달층 연구 개발은 소자의 효율 향상뿐만 아니라 소자의 안정성 개선도 기대 할 수 있다. 또한, LiF, Ca 등은 소자 제작을 위해서 진공 열 증착법을 이용하여 제작이 가능한데, 이는 소자 적용 분야의 제한을 가지고 온다.

증착방법은 설비를 갖추는데 설비자금이 매우 많이 들며, 증착을 하는 과정에서 소재의 낭비가 많은 등 대면적 코팅에 어려움이 있다. 그러므로 용액공정이 가능한 새로운 전자전달층의 개발은 다양한 이점을 가져올 수 있다.

일반적으로 전자전달 유기 물질은 n-type 구조를 가지고 있으며, 이는 보통 electron-deficient unit을 가지는 분자 구조로, triazine, quinoxaline, pyridine, oxidazole 등이 있다. 이와 같은 구조를 가지는 물질들이 전자전달물질로 연구되어 왔다. 그러나, hetero 방향족 화합물은 일반적으로 알코올 계열 용매에 낮은 용해도를 나타내어, 아래층 물질의 특성에 따라 용액 공정의 한계점이 나타난다. 일반적으로 넓은 에너지 밴드 갭을 가지는 전자전달물질은 OLED 소자에서 발광층과 전자전달층 사이의 에너지 장벽을 형성시켜 정공이 넘어가는 현상을 막아주어 OLED 소자에 적합하다.

본 연구는 위 내용을 바탕으로 electron deficient 구조로 잘 알려진 quinoxaline 유도체와 phosphine oxide 분자 구조를 이용하여 새로운 전자전달물질을 설계 및 합성을 하였다. Phosphine oxide 를 quinoxaline 구조에 도입하여 물질의 용해도 개선 및 넓은 에너지 밴드 갭을 가지는 물질을 개발하였으며, 더불어 전기 음성이 강한 phosphine oxide 를 이용하여 강한 dipole moment 를 가지는 소재를 개발하였다. 이를 통해 새로운 전자수송물질을 광전자 소자에 적용시켜 효율 향상을 기대하였다.

Chapter I. Introduction

I-1. Motivation

Organic light emitting diodes (OLEDs) and organic solar cells (OSCs) have been fascinating and investigated due to their attractive properties such as flexibility, low cost, and light weight for several decades. Also, OLEDs and OSCs are considered as promising candidates for the next generation display technology and green energy via their simple solution processing and roll to roll applications [1–7]. However, OLEDs and OSCs for commercial applications require remarkably efficient device performance as well as stability.

In order to reach the highly efficient devices, energy level alignment which suggests low energy barrier is required for efficient charge injection and extraction. Thus, the study of interlayer is significantly important for those optoelectronic devices [8–13]. The numerous electron-transporting materials have been developed to improve device performances. LiF and Ca of low work function of metallic compounds or ZnO and TiO_2 of n-type metal oxides, these cathode interlayer materials are widely used in optoelectronics for electron injection, transport, and extraction. The use of LiF and Ca become electron injection and extraction easier in devices due to lowered energy barrier

between active layer and electrode by tuning metal work function. In spite of their merits, LiF and Ca can be only deposited by vacuum thermal evaporation when its fabrication. There are two optoelectronic fabrication methods, vacuum thermal deposition and solution process. As people have known, vacuum thermal evaporation is such expensive methods and materials waste, on the other hand solution-processed fabrication is much useful and promising method due to low-cost and large-area coating application in optoelectronics. In addition, these alkali metal compounds exhibit inferior device stability to the moisture and oxygen. Thus, encapsulation is necessary to protect devices from ambient conditions [14]. Therefore, the study of new electron-transporting layers is worth to optoelectronic performances.

I-2. Organic Light-Emitting Diodes (OLEDs)

I-2-1. Background of OLEDs

Year	Event[a]	Company/Institute
1960–mid–1970s	D OLED crystal molecule, anthracene, etc.	NRC (Canada), RCA
1987	P OLED diode structure paper in *Appl. Phys. Lett.*	Eastman Kodak
1990	P first PLED paper in *Nature*	Cambridge Univ.
1996	P first AMOLED demonstration (QVGA)	TDK
1998	D first phosphorescence OLED	Princeton Univ.
1999	D first passive OLED product	Pioneer
2001	D 0.72-in. headmount display by AMOLED on silicon	eMagin
2001	D 13-in. SVGA AMOLED prototype	Sony
2001	D 2.1-in. 130-ppi AMOLED prototype	Seiko Epson/CDT
2002	D 15-in. 1280 × 720 OLED prototype	Eastman Kodak/Sanyo
2003	D digital camera with 2.2-in. AMOLED display	Eastman Kodak
2003	D Tiled 24-in. AMOLED prototype with by 12-in. display	Sony
2003	D 20-in. phosphorescence AMOLED prototype by a-Si backplane	ChiMei/IDT/IBM

[a]*Abbreviations in this column*: a-si—amorphous silicon; AMOLED—active-matrix OLED; D—development of; P—publication or presentation/demonstration of; PLED—polymer (O)LED; ppi—pixels per inch; QVGA—quarter videographics array (320 × 240 pixels); SVGA—super videographics array (800 × 600 pixels).
Source: SID International Symposium (2003), 40 Years of SID Symposia—Nurturing Progress in EL/OLED Technology, Baltimore, MD.
http://www.sid.org/Archives.aspx

Figure I-1. History of OLEDs [15].

Since discovery of electroluminescence (EL) from organic molecules, EL materials were gradually interesting in research field. The first discovery of EL was from organic materials by applying alternating-current (AC) fields. André Bernanose found its phenomenon at Nancy University in France in the

early 1950s [16, 17]. Then in 1960, Martin Pope and his team developed ohmic dark-injecting electrode contacts to organic crystals and characterized the basis of charge injection in modern OLED devices [18, 19]. They also observed direct-current (DC) EL on a single crystal of anthracene [20]. After discovery of EL of organic materials, Ching W. Tang and Steven Van Slyke developed the first working OLED in 1987 [21], as shown in Figure I-1. Since the first working OLED emerged, OLEDs have been intensively explored and investigated because of their advantages, which contain cost-effective, versatile molecular design, flexible mechanical property, and large-area fabrication via simple solution process. Hence, OLEDs are considered as one of the promising candidates for the next generation display technology and solid-state lighting.

I-2-2. Development of OLEDs structure

As first single layer OLEDs emerged, mono layer device comprised emissive layer between emissive layer and electrodes. Simply, a low work function (WF) of metal cathode and a high WF of transparent anode (Indium Tin Oxide, ITO) are used in OLEDs. Holes and electrons injected from electrodes toward

the organic layer by the high electric field and recombine to be exciton. However, single layer OLEDs exhibit very poor device performances with low luminous efficiency (LE) due to its large energy barrier between organic layer and electrodes. Hence, the device structure has been much developed as double layers and multi layers OLEDs. The multilayer OLEDs composed of anode, hole-transporting layer (HTL), organic-emitting layer, electron-transporting layer (ETL), and cathode as shown in Figure I-2.

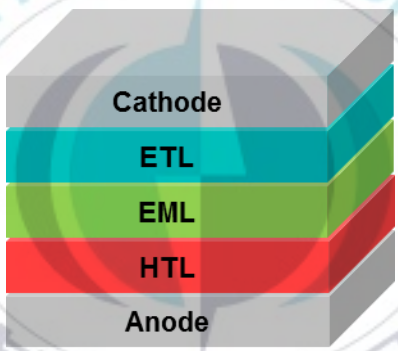

Figure I-2. Multilayer OLED device structure.

I-2-3. Physical mechanism of OLEDs

Figure I-3 shows the fundamental operating mechanism of OLED device. OLEDs generate the photon energy in response to electrical currents from organic semiconductors. When the electrical current is applied on OLEDs, OLEDs can emit the light, which called electroluminescence. According to

electrical energy source, holes and electrons are injected into an organic layer, and then organic material can be emitting the light.

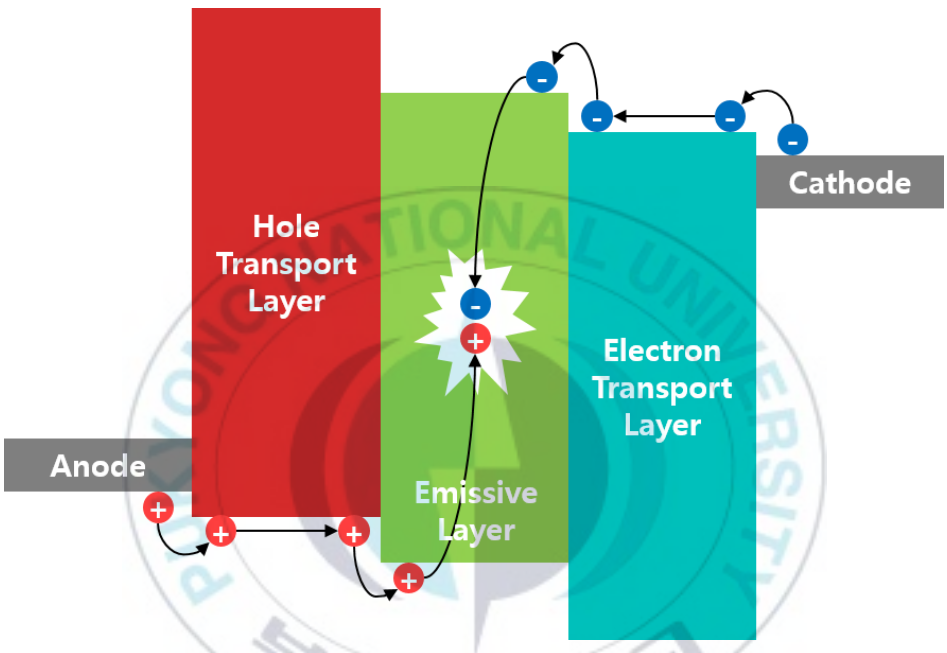

Figure I-3. Operational principle of OLEDs.

Operating mechanism of OLEDs can be explained through charge injection, charge transport, recombination, and light emission [15].

[1] Charge injection

When the electric field is applied to the OLED device, holes and electrons are injected from anode and cathode respectively toward organic emissive

layer. For electron injection, low WF materials such as LiF, Ca are generally used onto cathode layer. ITO with high WF is used as transparent anode for hole injection. Holes are injected to the HOMO of the emissive layer meanwhile electrons are injected to the LUMO of the emissive layer through each electrode. LiF/Al cathode configuration is frequently used as electron injection layer of OLED devices, which known as electron injection through the vacuum level shift. LiF is such a significant agent to improve the electron injection from Al to organic materials, so it is one of the most powerful cathode interlayer. Hence, energy level alignment which suggests lower energy barrier between organic layer and electrodes is required for efficient charge injection, leading to improvement of device efficiency.

[2] Charge transport

When the electric field is applied, charges are injected to HTL and ETL from each electrode. The charge mobility character is most important properties for HTL and ETL. Each transport layer transports charges toward the recombination sites such as organic emissive layer. In order to increase device efficiencies, well-matched holes and electrons transport is demanded. According to

mobility characters, balanced charge transport can be controlled by introducing of HTL and ETL.

[3] Recombination and light emission

The recombination of hole and electron generates the exciton, the exciton formation mainly affects to the device performances. The charge injection and transport are the most important factor of efficient recombination of hole and electron. Furthermore, charge blocking layer is required to both sides of emissive layer for exciton confinement. This leads to enhancing the number of recombination. The generated exciton via charge recombination can be light emission. According to the quantum mechanical rules, 25% of excitons create singlets and 75% of triplets created. Fluorescent material of organic emissive layer generates singlet exciton, on the other hand phosphorescent material creates both singlet and triplet excitons.

[4] Emission

The working principle of light-emitting diodes is based on the generation of excitons, which created by charge recombination. According to the quantum mechanical rules, 25% of excitons create singlets and 75% of triplets created.

Fluorescent material of organic emissive layer generates singlet exciton, on the other hand phosphorescent material creates both singlet and triplet excitons.

I-2-4. Characterization of OLEDs

For characterization of OLEDs, the main parameters have mentioned such as turn-on voltage, luminance, luminous efficiency (LE), and external quantum efficiency (EQE). Turn-on voltage is the minimum voltage required for injection of holes and electrons, when the minimum luminance is at 0.1cd/m^2. This mostly depends on the energy levels of organic materials and electrodes.

To the device efficiency, the internal quantum efficiency (IQE) is calculated as the ratio of the number of photons generated in the cell to the number of electrons in the external circuit. The IQE is determined by the following formula:

$$\eta_{int} = \gamma \cdot r_{st} \cdot \varphi$$

Where γ is the ratio of the number of exciton creation in the cell to the number of electrons flowing in the external circuit, r_{st} is the fraction of singlet exciton φ is the efficiency of radiative decay of singlet excitons.

The external quantum efficiency (EQE) is calculated as the ratio of the

number of photons emitted from the OLED cell to the number of injected electrons. The EQE is determined by the following formula:

$$\eta_{ext} = \eta_{int} \cdot \eta_{extr} = \gamma \cdot r_{st} \cdot \varphi \cdot \eta_{extr}$$

Where η_{extr} is the light extraction efficiency from OLEDs, which is the total internal reflection loss.

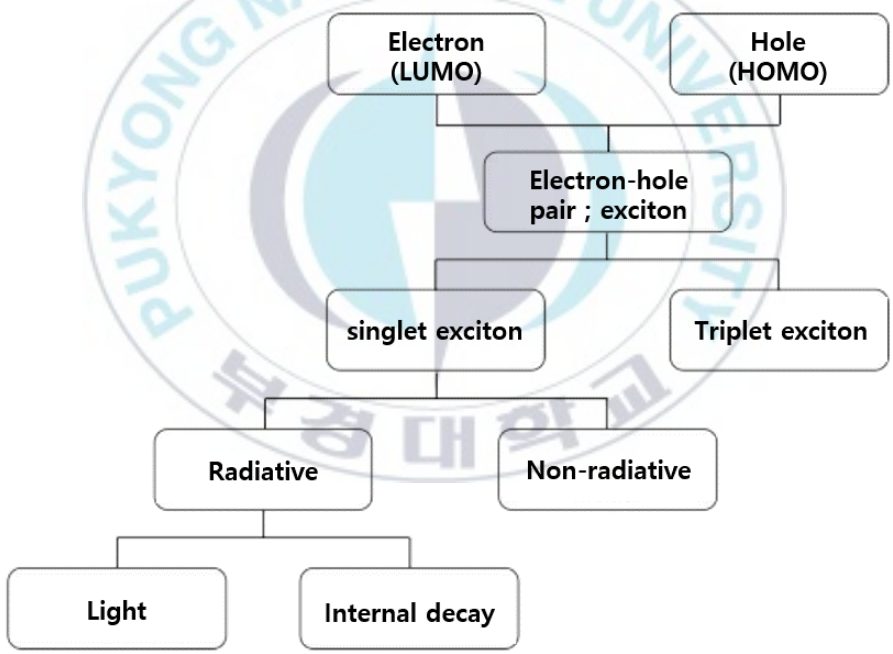

Figure I-4. Schematic EL process with efficiency parameters.

I-3. Organic solar cells (OSCs)

I-3-1. Background of OSCs

The energy consumption is dramatically growing fast all over the world. However, limited energy sources such as coal, natural gas, and oil have become big problems nowadays. These limited energy issues have been attractive to people and helped advanced countries and scientists have interests in developing new energy sources. In order to solve the energy issues, many people put their efforts to study on renewable energy such as hydrogen, bio-energy, geothermal energy, and solar energy. Among various alternative energy sources, solar energy is one of the promising candidates due to its excellent merits, infinite energy sources, and easy access.

Since the first photovoltaic effect is reported by Becquerel in 1839, the study of organic solar cells has been intensively developed for new organic active layer over the past two decades. OSCs has been greatly grown due to many efforts and interests, improved good materials and process techniques for highly efficient devices. Recently, the photovoltaic performance has reached about 15% of power conversion efficiency (PCE) based on OSC device [22].

I-3-2. Device structure of OSCs

Bulk heterojunction (BHJ) OSCs is one of promising method to fabricate photovoltaic device. Blended donor material, benzodithiophene (BDT)-based PTB7-Th, and acceptor, fullerene derivatives, as a blended active layer was sandwiched between a transparent anode (indium tin oxide (ITO)) and low work function metal (LiF, Ca and Al). Also, hole transport and electron transport layers inserted between active layer and each electrode.

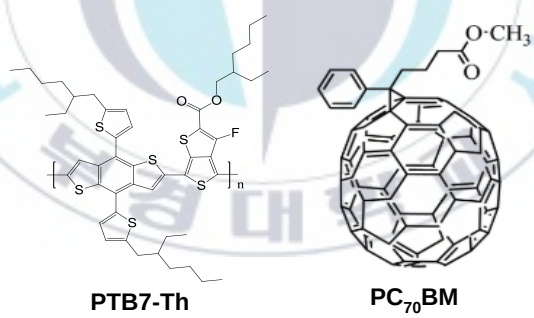

Figure I-5. Chemical structures of BDT-based donor (PTB7-Th) and fullerene-based acceptor ($PC_{70}BM$).

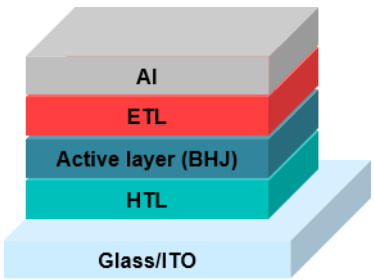

Figure I-6. OSC device structure.

I-3-3. Physical mechanism of OSCs

Figure I-7 shows the fundamental operating mechanism of OSC device, which is explained via four steps. First, excitons can be created by light absorption of donor. Next, excitons are dissociated at the interface of donor and acceptor. The exciton separation is able to happen within the exciton diffusion length (around 10nm). After electron-hole pairs being separated, holes and electrons move to donor and acceptor network, respectively. Finally, the dissociated holes and electrons are collected at the anode and cathode, respectively .

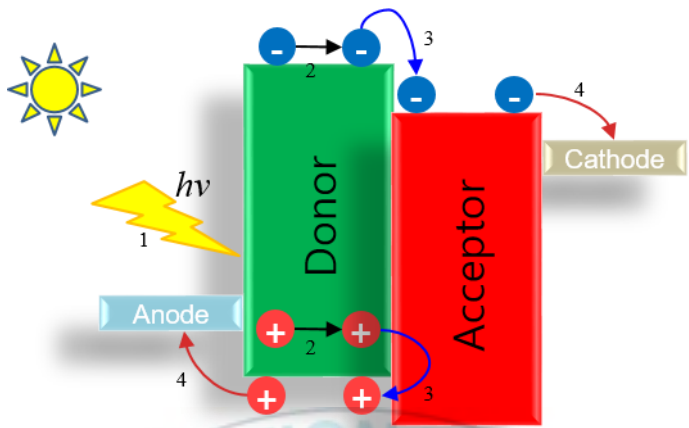

Figure I-7. Operational principle of D-A heterojunction solar cell.

[1] Light absorption and exciton formation

The photovoltaic properties are strongly related to the optical properties of organic semiconductors. They can generate a pair of electron and hole induced by light absorption when the photon energy is equal or stronger than the band gap. The sunlight is absorbed through active layer of BHJ-OSC devices, the semiconductor of active materials, donor and acceptor, can be excited and generate excitons by photoexcitation.

[2] Exciton diffusion

After the generation of the exciton, it can be separated at the interface of the donor and acceptor. Owing to its short diffusion length, before dissociated

exciton, it might be decayed. The exciton should move to the interface within the range of diffusion length, exciton diffusion length has a critical influence in photovoltaic properties in OSCs.

[3] Exciton dissociation

When the exciton reaches to the interface of the donor and acceptor, electron-hole pairs dissociated as free charges. The exciton separation is efficiently occurred by the energy difference around 0.3eV between LUMO of the donor and LUMO of the acceptor, due to exciton binding energy.

[4] Charge transport and collection

Once free charges are generated, they move through the networks of donor and acceptor, and transfer to each electrode.

I-3-4. Characterization of OSCs

For characterization of OSCs, the main parameters are mentioned as open circuit voltage (V_{oc}), short circuit current (J_{sc}), and fill factor (FF). The power conversion efficiency (PCE) is determined by these factors and the following formula:

$$PCE = \frac{V_{oc}\ x\ J_{sc}\ x\ FF}{P_{in}}$$

(P_{in} is incident light power density)

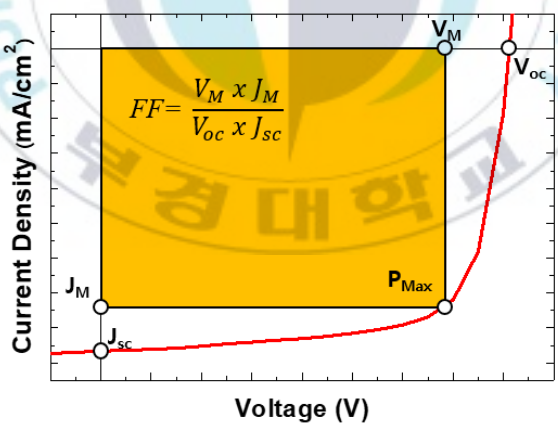

Figure I-8. J-V curves of OSCs.

[1] Open circuit voltage (V_{oc})

The open circuit voltage (V_{oc}) is the maximum voltage when disconnected state. The V_{oc} is mostly related to the energy difference between the highest occupied molecular orbital (HOMO) of donor and the lowest unoccupied molecular orbital (LUMO) of acceptor at the interface of donor and acceptor.

[2] Short-circuit current density (J_{sc})

The short-circuit current (J_{sc}) is the current flows through device when the voltage across the solar cell is zero. The J_{sc} is the maximum current density and determined by exciton creation from absorption of sun light in active layer.

[3] Fill factor (FF)

The fill factor (FF) is the ratio of the actual power of solar cell and determined by V_M, J_M, V_{oc}, and J_{sc}. Here V_M and J_M are the voltage and current density at the maximum power respectively. The FF is related to many factors such as active layer morphology, charge carrier mobility, and charge recombination.

$$FF = \frac{V_M \ x \ J_M}{V_{oc} \ x \ J_{sc}}$$

I-4. Molecular design of electron transport materials

For the past decades, organic electron-transporting materials have been designed and synthesized with different structures and features for improving optoelectronic performances. Basically, electron-transporting materials are consisting of n-type structure considered as electron-deficient units, hetero-aromatics, such as triazine, quinoxaline, pyridine, oxidazole, phenanthroline, etc. These electron-deficient units have been generally investigated for electron-transporting materials for the performances of optoelectronics[23–27]. However, hetero-aromatic compounds usually exhibit poor solubility in alcohol which restricts solution-processed devices, depending on the bottom layer. Normally wide energy bandgap (E_g) material is preferred for ETLs in OLEDs because of hole blocking behavior when the charge move to next layer from emissive layer to ETL, charge transporting is quite difficult due to its energy barrier. However, extending π-conjugation system may cause a narrow E_g. Due to metal cathodes with high work functions such as 4.3 eV of Al, a thin internal layer of LiF is usually deposited before the metal cathodes in order to lower energy barrier between emissive layer and electrodes. Therefore, the study of interfacial dipoles may be important for electron-transporting materials.

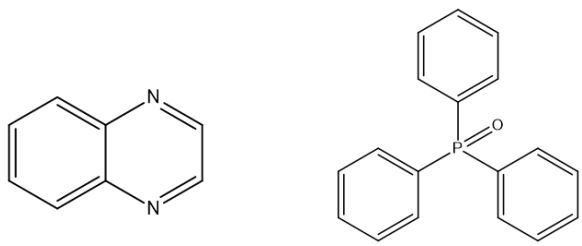

Quinoxaline Phosphine oixde

Figure I-9. Chemical structure of quinoxaline and phosphine oxide

Herein, we designed and synthesized new electron-transporting materials which consist of quinoxaline and phosphine oxide moieties, QxTPPO and QxTPPO2, which considered as N-type organic compounds. Quinoxaline derivative has been chosen for well electron-transporting and the phenyl rings are placed at 2,3-position of quinoxaline moiety. In order to solve the limitation of application in solution processed devices, Phosphine oxide group (P=O) has been introduced to the quinoxaline derivative for soluble in alcohol. According to electron negativity, the strong dipole moment of phosphine oxide forms electron density deviation within the molecular structure depending on the physical architecture of the molecules. Specific molecular geometries can be strongly polar so that introducing phosphine oxide group can make the molecules soluble in polar solvent such as methanol, isopropyl alcohol. Phos-

phine oxide-based structures (QxTPPO, QxTPPO2) produce permanent dipole between active layer and cathode, accordingly we expected cathode work function will be tuned. In addition, compared to other functional groups, phosphine oxide does not extend the conjugation system because the phosphine oxide unit interrupts the conjugated connection [28–33]. Consequently, new electron-transporting materials, QxTPPO and QxTPPO2, were successfully synthesized and explored in this study. Qx ETLs can not only used in OLED, but also in OSC because of its significant electron-transporting properties.

Chapter II. Experimental section

II-1. Materials and instruments

Benzothiadiazole, benzil, 9,10-phenanthrenequinone, chlorodiphenylphosphine, and all the other materials were purchased from Sigma-Aldrich and TCI, used as received without purification. ^{1}H, ^{13}C, and ^{31}P NMR spectra were recorded on a JEOL JNM ECA 600 spectrometer. UV-vis spectra were recorded using a JASCO V-530 UV-vis spectrophotometer. Gas chromatography mass spectroscopy (GC-MS) was conducted using Bruker 450-GC & 320-MS spectrometer. Cyclic voltammetry (CV) measurements were carried out using a VersaSTAT3 potentiostat (Princeton Applied Research) in tetrabutylammonium hexafluorophosphate (0.1M, Bu_4NPF_6) as the electrolyte in acetonitrile. For CV measurements, a glassy carbon electrode coated with a thin layer of small molecules and platinum wire were used as the working and counter electrode, respectively. A silver wire was used as a pseudo-reference electrode with a ferrocene/ferrocenium external standard.

II-2. Synthesis of organic small molecules

II-2-1. (4-Bromophenyl)diphenylphosphine (2)

1,4-Dibromobenzene (1) (5g, 21.2mmol) was prepared in vacuumed flask and refilled nitrogen. 100ml of THF was added, cooled temperature at -78˚C, 30min later n-Butyllithium (2.5M, 9.4ml, 23.5mmol) was added dropwise and stirred for 30min. Chlorodiphenylphosphine (4.2ml, 23.3mmol) was added to this solution and stirred for 1h, then the reaction was allowed to warm to room temperature, and continued to stir overnight. The reaction was evaporated under reduced pressure, crude mixture was extracted with dichloromethane, dried over magnesium sulfate, and filtered. The filtrate was removed under reduced pressure, and purified with column chromatography (hexane). Product was obtained as white solid with 90% of yield. ^{1}H-NMR (600 MHz, $CDCl_3$): δ = 7.45 (dd, *J* = 8.28, 1.38 Hz, 2H), 7.35-7.31 (m, 6H), 7.3-7.26 (m, 4H), 7.14 (m, 2H). ^{13}C-NMR (150 MHz, $CDCl_3$): δ = 136.7, 136.6, 135.3, 135.2, 133.8, 133.7, 131.78, 131.74, 129.0, 128.77, 128.72, 128.6, 128.5, 123.4. ^{31}P-NMR (243 MHz, $CDCl_3$): δ = -5.76.

II-2-2. Diphenyl(4-(4,4,5,5-tetramethyl-1,3,2-dioxaborolan-2-yl)phenyl)phosphine (3)

(4-Bromophenyl)diphenylphosphine (2) (2g, 5.86mmol), bis(pinacolato)-diboron (1.8g, 7.09mmol), potassium acetate (1.4g, 14.1mmol), $Pd(dppf)Cl_2$ (5% mol). All reagents was prepared in flask, vacuumed, and refilled nitrogen. Toluene (30ml) was added, the reaction was carried at 100˚C refluxed under N_2 for 24h. Mixture extracted with dichloromethane, dried over magnesium sulfate, and filtered. The filtrate was removed under reduced pressure, and purified with column chromatography (dichloromethane / hexane, 1/2). Product was obtained as crystalline solid (60%). ^{1}H-NMR (600 MHz, $CDCl_3$): δ = 7.75 (m, 2H), 7.35-7.29 (m, 12H), 1.33 (s, 12H). ^{13}C-NMR (150 MHz, $CDCl_3$): δ = 141.3, 141.2, 137.2, 137.1, 134.97, 134.92, 134.1, 134.0, 133.1, 133.0, 129.0

II-2-3. Diphenyl(4-(4,4,5,5-tetramethyl-1,3,2-dioxaborolan-2-yl)phenyl)phosphine oxide (4)

Diphenyl(4-(4,4,5,5-tetramethyl-1,3,2-dioxaborolan-2-yl)phenyl)phos-

phine (3) (1g, 2.58mmol) was dissolved in dichloromethane (30ml). Hydrogen peroxide, 30% aqueous H_2O_2, (10ml) was added in the solution and the mixed solution was stirred at room temperature for three hours. The mixed solution was poured into water and extracted with dichloromethane and dried over magnesium sulfate and filtered. The filtrate was removed under reduced pressure, and purified with column chromatography (ethyl acetate / hexane, 4/1). White crystal solid was obtained as product (98%). ^{1}H-NMR (600 MHz, $CDCl_3$): δ = 7.89 (dd, *J* = 8.22, 3.43 Hz, 2H), 7.70-7.62 (m, 6H), 7.54 (m, 2H), 7.45 (m, 4H), 1.34 (s, 12H). ^{13}C-NMR (150 MHz, $CDCl_3$): δ = 135.5, 134.8, 134.6, 134.5, 132.8, 132.2, 132.1, 132.04, 132.03, 131.3, 131.2, 128.6, 128.5, 84.2, 24.9 ^{31}P-NMR (243 MHz, $CDCl_3$): δ = 29.64.

II-2-4. 4-Bromo-2,1,3-benzothiadiazole (6)

2,1,3-Benzothiadiazole (5) (5g, 36.76mmol) was dissolved in 48% HBr (80ml) at 150˚C. Bromine (1.69ml, 33.1mmol) was added dropwise via a dropping funnel. The reaction was conducted at 150˚C and refluxed for 2h. Then reaction cooled to room temperature and quenched with $NaHSO_3$ solution, then poured into water (300ml), extracted with MC. Organic phase was dried over magnesium sulfate, and filtered. The filtrate was removed under

reduced pressure. Mixture was purified with column chromatography (dichloromethane / hexane, 1/5) and further purification using hexane by recrystallization. A pale solid was obtained as product (70%). ^{1}H-NMR (600 MHz, $CDCl_3$): δ = 7.97 (dd, *J* = 8.58, 1.02 Hz, 1H), 7.83 (d, 1H), 7.47 (m, 1H). ^{13}C-NMR (150 MHz, $CDCl_3$): δ = 154.6, 153.3, 132.0, 129.9, 120.9, 114.4.

II-2-5. 4,7-Bromo-2,1,3-benzothiadiazole (7)

2,1,3-Benzothiadiazole (5g, 36.76mmol) was dissolved in 48% HBr (80ml) at 150˚C. Bromine (3.8ml, 74.43mmol) was added dropwise through a dropping funnel. The reaction was conducted at 150˚C and refluxed for 2h. After 2h reaction, cooled to room temperature and quenched with $NaHSO_3$ solution, then poured into water (300ml), extracted with MC. Organic phase was dried over magnesium sulfate, and filtered. The filtrate was removed under reduced pressure. Crude mixture was purified with column chromatography (dichloromethane / hexane, 1/5) and further purification using hexane by recrystallization. A pale solid was obtained as product (78%). ^{1}H-NMR (600 MHz, $CDCl_3$): δ = 7.72 (s, 2H). ^{13}C-NMR (150 MHz, $CDCl_3$): δ = 152.9, 132.3, 113.9.

II-2-6. 5-Bromo-2,3-diphenylquinoxaline (8)

4-Bromo-2,1,3-benzothiadiazole (6) (2g, 9.3mmol) was dissolved in ethanol (100ml). $NaBH_4$ (6.51g, 172mmol) was added in the solution slowly as three portions. The reaction was kept at 0˚C for a while, then the reaction was allowed to warm to room temperature and stirred overnight. The solution was evaporated under reduced pressure, and crude mixture was extracted with ether, dried over magnesium sulfate, and filtered. The filtrate was removed under reduced pressure. Crude mixture was dissolved in ethanol (40ml) and acetic acid (40ml) as co-solvents, benzil (2.35g,11.17mmol) was added. The mixture was heated at 110˚C for overnight. Solution was poured into water, extracted with MC, dried over magnesium sulfate, and filtered. Organic solvent was removed under reduced pressure. Organic mixture was purified with column chromatography (dichloromethane / hexane, 1/5). White solid of product was obtained (50%). ^{1}H-NMR (600 MHz, $CDCl_3$): δ = 8.13 (dd, *J* = 8.04, 1.02 Hz, 1H), 8.07 (dd, *J* = 7.56, 1.5 Hz, 1H), 7.62 (m, 3H), 7.55 (m, 2H), 7.41-7.33 (m, 6H). ^{13}C-NMR (150 MHz, $CDCl_3$): δ = 154.0, 153.7, 141.9, 138.9, 138.7, 138.4, 133.3, 130.3, 130.1, 129.9, 129.3, 129.2, 129.0, 128.5, 128.3, 124.2.

II-2-7. 5,8-Dibromo-2,3-diphenylquinoxaline (9)

4,7-Dibromo-2,1,3-benzothiadiazole (1g, 3.4mmol) was dissolved in ethanol (50ml). $NaBH_4$ (2.38g, 62.9mmol) was added in the solution slowly as three portions. The reaction temperature was treated using ice to set 0˚C for a while, then the reaction was allowed to warm to room temperature and stirred overnight. The mixture was evaporated under reduced pressure, and crude mixture was extracted with ether, dried over magnesium sulfate, and filtered. The filtrate was removed under reduced pressure. Crude mixture was dissolved in ethanol (40ml) and acetic acid (20ml) as co-solvents, benzil (0.86g, 4.08mmol) was added. Mixture was heated at 110˚C for overnight. The mixture solution was poured into water, extracted with MC, dried over magnesium sulfate, and filtered. Organic solvent was removed under reduced pressure. Organic mixture was purified with column chromatography (dichloromethane / hexane, 1/5). White solid of product was obtained (64%). ^{1}H-NMR (600 MHz, $CDCl_3$): δ = 7.92 (s, 2H), 7.66 (d, 4H), 7.41 (t, 2H), 7.36 (t, 4H). ^{13}C-NMR (150 MHz, $CDCl_3$): δ = 154.2, 139.4, 138.0, 133.1, 130.3, 129.6, 128.4, 123.8.

II-2-8. Synthesis of QxTPPO

5-Bromo-2,3-diphenylquinoxaline (1mmol) and Diphenyl(4-(4,4,5,5-tetramethyl-1,3,2-dioxaborolan-2-yl)phenyl)phosphine oxide (1mmol) were dissolved in dry toluene (12ml). After degassing with N_2 for 15min, $Pd(PPh_3)_4$ (5mol%) and 2M K_2CO_3 (5ml) were added in a schlenk flask. The reaction mixture was heated and stirred at 90˚C for 48h under N_2 atmosphere. Upon completion of the reaction, the reaction mixture was poured into water and extracted with dichloromethane. Organic phase was separated and dried over magnesium sulfate. After removal of solvent under reduced pressure, the crude residue was purified with column chromatography (ethyl acetate / dichloromethane, 1/2). Further purification is processed using the combination of ethyl acetate and hexane by recrystallization. White solid of product was obtained (57%). ^{1}H-NMR (600 MHz, $CDCl_3$): δ = 8.19 (m, 1H), 7.92 (dd = 8.22, 2.04 Hz, 2H), 7.83-7.73 (m, 8H), 7.56 (m, 4H), 7.48 (m, 6H), 7.36 (m, 3H), 7.31 (t, 1H), 7.26 (t, 2H). ^{13}C-NMR (150 MHz, $CDCl_3$): δ = 153.2, 152.6, 142.1, 142.0, 141.2, 139.2, 139.1, 138.78, 138.73, 132.3, 132.2, 132.0, 131.8, 131.7, 131.09, 131.01, 130.1, 129.8, 129.4, 128.6, 128.5, 128.4, 128.2. ^{31}P-NMR (243 MHz, $CDCl_3$): δ = 29.83. GC-MS: m/z calcd, 558.608; found, 588.2 [M^+].

II-2-9. Synthesis of QxTPPO2

5,8-Dibromo-2,3-diphenylquinoxaline (1mmol) and Diphenyl(4-(4,4,5,5-tetramethyl-1,3,2-dioxaborolan-2-yl)phenyl)phosphine oxide (2mmol) were dissolved in dry toluene (12ml). After degassing with N_2 for 15min, $Pd(PPh_3)_4$ (5mol%) and 2M K_2CO_3 (5ml) were added in a schlenk flask. The reaction mixture was heated and stirred at 90˚C for 48h under N_2 atmosphere. Upon completion of the reaction, the reaction mixture was poured into water and extracted with dichloromethane. Organic phase was separated and dried over magnesium sulfate. After removal of solvent under reduced pressure, the crude residue was purified with column chromatography (ethyl acetate / dichloromethane, 1/2). Further purification is processed using the combination of ethyl acetate and hexane by recrystallization. White solid of product was obtained (64%). ^{1}H-NMR (600 MHz, $CDCl_3$): δ = 7.95 (dd = 8.28, 2.76 Hz, 2H), 7.89 (s, 1H), 7.83 (dd = 11.7, 8.22 Hz, 2H), 7.76 (m, 4H), 7.56 (m, 4H), 7.49 (m, 4H), 7.34 (t, 1H), 7.28 (t, 2H). ^{13}C-NMR (150 MHz, $CDCl_3$): δ = 152.0, 141.8, 139.1, 138.7, 138.5, 133.0, 132.35, 132.30, 132.2, 132.0, 131.89, 131.82, 131.1, 131.0, 130.9, 130.1, 130.0, 129.2, 128.68, 128.60, 128.3. ^{31}P-NMR (243 MHz, $CDCl_3$): δ = 29.62. GC-MS: m/z calcd, 834.877; found, 834.8 [M^+].

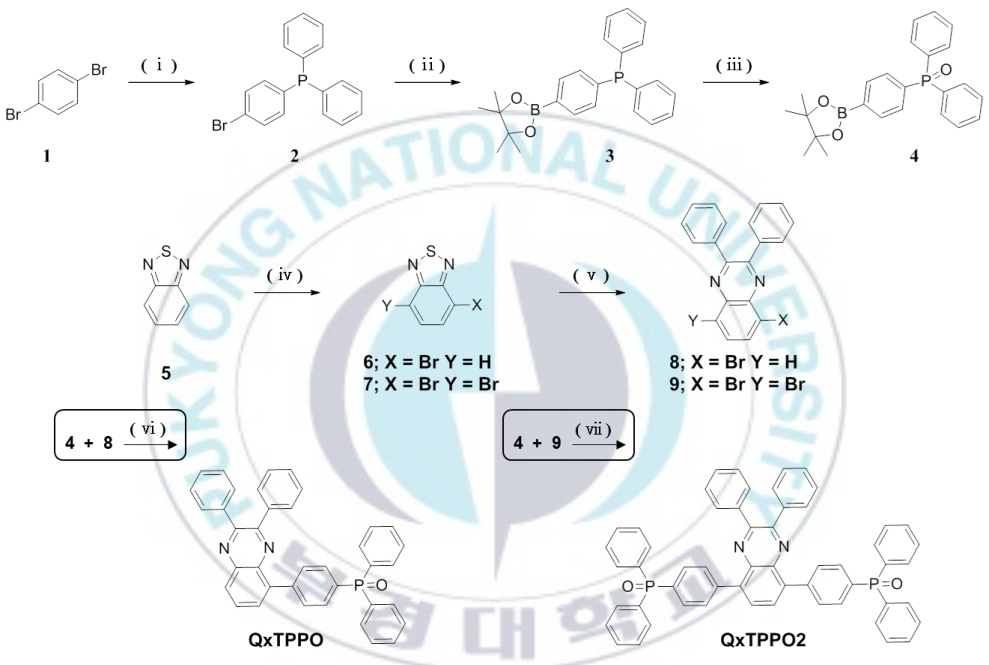

Scheme 1. Synthetic route of QxTPPO and QxTPPO2

II-3. Fabrication of optoelectronic devices

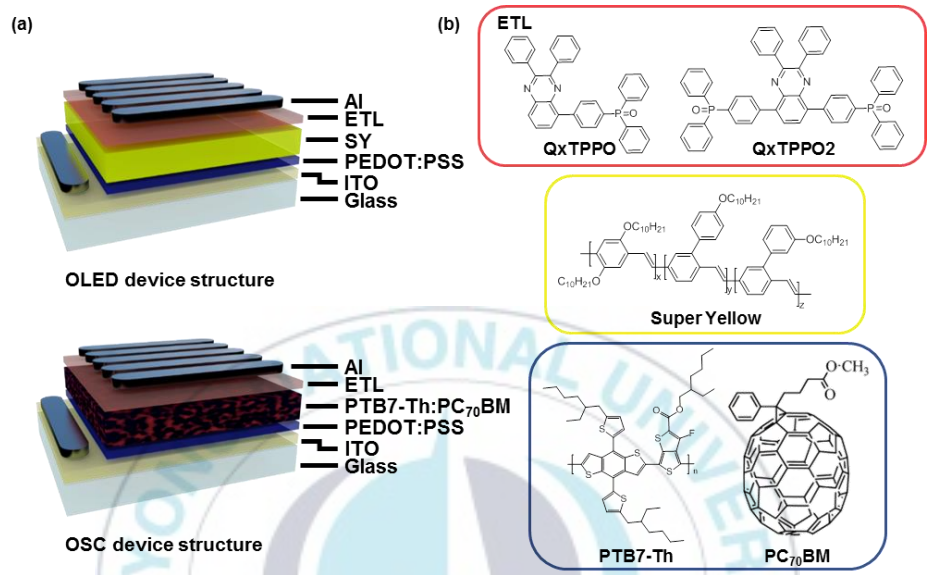

Figure II-1. Optoelectronic device and chemical structures (a) Device architectures of OLED and OSC, (b) Chemical structures of ETLs and active materials for OELD and OSC.

OLED device was fabricated on patterned ITO-coated glass substrates, which cleaned by sequential ultrasonic treatments in acetone and isopropyl alcohol (IPA). After UV-ozone treatment, poly(3,4-ethylenedioxythiophene):poly-(styrenesulfonate) (PEDOT:PSS, AI 4083, Clevios) solution (filtered through a 0.45μm PVDF filter) was spin-coated at 2500 rpm for 45s onto ITO substrate then baked at 150˚C for 10min. Poly(*para*-

phenylenevinylene) known as “Super Yellow” (SY, Merck Co., M_w = 1,950,000 g/mol) solution dissolved in chlorobenzene (0.7 wt%) was spin-cast at 2000rpm on top of the PEDOT:PSS to obtain 150 nm thick SY layer. Finally, Qx ETLs were spin-cast at 3000rpm, and 100nm of Al layer was thermally deposited.

OSC device was also fabricated same as OLED device fabrication. After UV-ozone treatment, poly(3,4-ethylenedioxythiophene):poly-(styrenesul-fonate) (PEDOT:PSS, AI 4083, Clevios) solution (filtered through a 0.45μm PVDF filter) was spin-coated at 2500 rpm for 45s onto ITO substrate then baked at 150˚C for 10min. A solution of poly[4,8-bis[5-(2-ethylhexyl)-2-thienyl]benzo[1,2-b:4,5-b′]dithiophene-alt-(4-(2-ethylhexyl)-3-fluorothieno[3,4-b]thiophene-)-2-carboxylate-2- 6-diyl)] (PTB7-Th) and [6,6]-phenyl C70-butyric acid methyl ester (PC70BM) (1:1.5) in chlorobenzene : 1,8-diiodooctane (DIO) (97:3 vol%) were then spin-cast on top of the PEDOT:PSS layer. The BHJ film was dried for 30min at room temperature in a glove box. Finally, Qx ETLs were spin-cast at 3000rpm, and 100nm of Al layer was thermally deposited.

Chapter III. Results and Discussion

III-1. Characterization of organic small molecules

III-1-1. Thermal properties

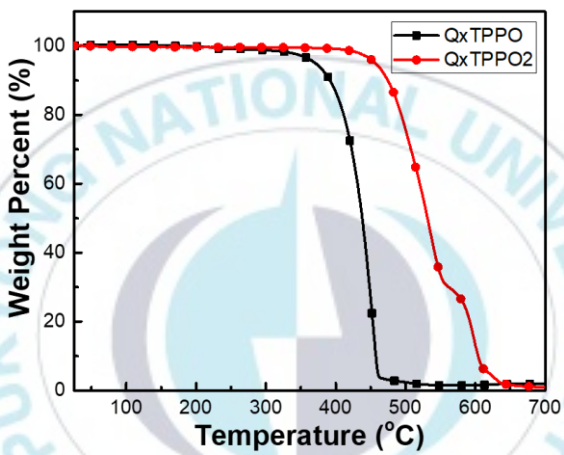

Figure III-1. TGA thermograms of QxTPPO and QxTPPO2 at a heating rate of 10˚C/min under air

The thermal properties of QxTPPO and QxTPPO2 have been investigated using thermogravimetric analysis (TGA). The TGA measurement was conducted at a heating rate 10˚C/min under the ambient condition, the results are shown in Figure III-1. Two organic small molecules showed good thermal stability with 370.8˚C and 456.9˚C of decomposition temperature 5 wt % loss

($T_{d5\%}$) respectively.

III-1-2. Optical and electrochemical properties

The UV-vis absorption spectra of QxTPPO and QxTPPO2 in diluted $CHCl_3$ solution and in film state are shown in Figure III-2. These organic small molecules exhibit ultraviolet range absorption from 400nm. The optical band gap has been explored via film state UV-vis spectra, 3.1eV of QxTPPO and 2.97eV of QxTPPO2 were obtained. Meanwhile, these small molecules exhibit similar maximum absorption coefficients. According to the chemical architecture, symmetric molecule (QxTPPO2) shows red-shifted absorption band compared to asymmetric molecule (QxTPPO), which means additional phenyl ring of triphenylphosphine oxide contributes relatively longer conjugation length. The electrochemical properties of small molecules were investigated by cyclic voltammetry. The highest occupied molecular orbital (HOMO) and the lowest unoccupied molecular orbital (LUMO) of QxTPPO and QxTPPO2 were confirmed to be -3.0eV, -3.06eV of LUMO and -6.22eV, -6.17eV of HOMO energy level from onset potential respectively. This low HOMO energy level of Qx materials can sufficiently block holes form various

active materials. 3.21eV and 3.11eV of the electrochemical bandgap were calculated via cyclic voltammetry (see in Figure III-3), we can also see the symmetric molecule of QxTPPO2 exhibits smaller band gap. In addition, the detail information of optical and electrochemical properties has been listed in Table III-1. The energy diagrams of OLED and OSC with Qx ETL series are shown in Figure III-4.

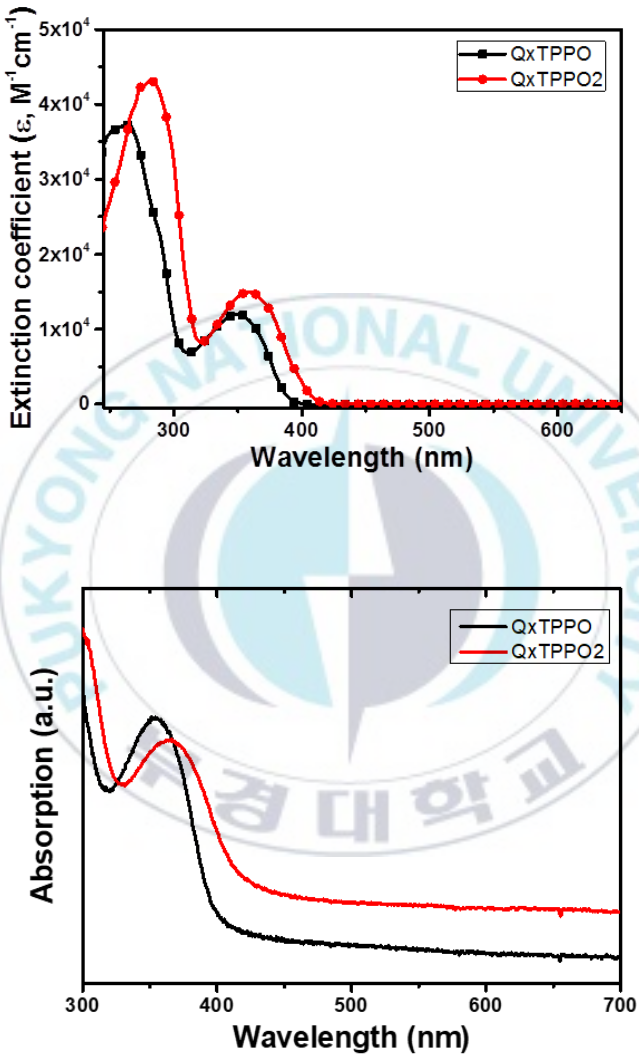

Figure III-2. UV-vis spectra of QxTPPO and QxTPPO2 in chloroform solution and film on the glass substrate

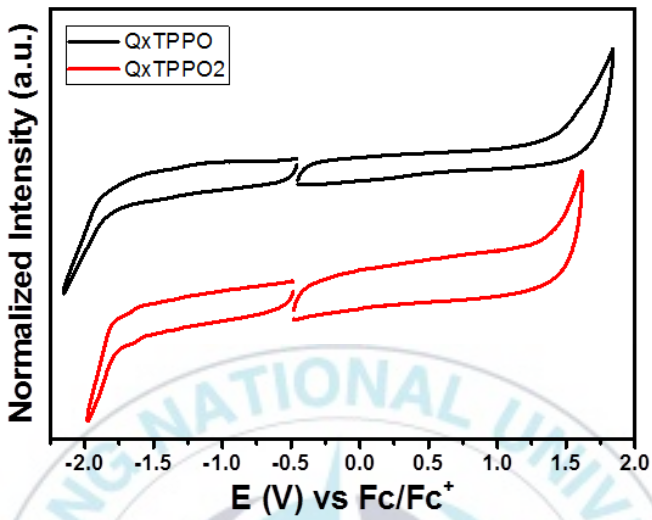

Figure III-3. Cyclic voltammetry of QxTPPO and QxTPPO2

Table III-1. Summary of optical and electrochemical properties of the organic small molecules

	ε (10^5 $M^{-1}cm^{-1}$)	λ_{max}^{sol} (nm)	λ_{edge}^{film} (nm)	LUMO (eV)	HOMO (eV)	E_g^{opt} (eV)	E_g^{cv} (eV)
QxTPPO	3.731	265	399	3.00	6.22	3.10	3.21
QxTPPO2	4.327	282	417	3.06	6.17	2.97	3.11

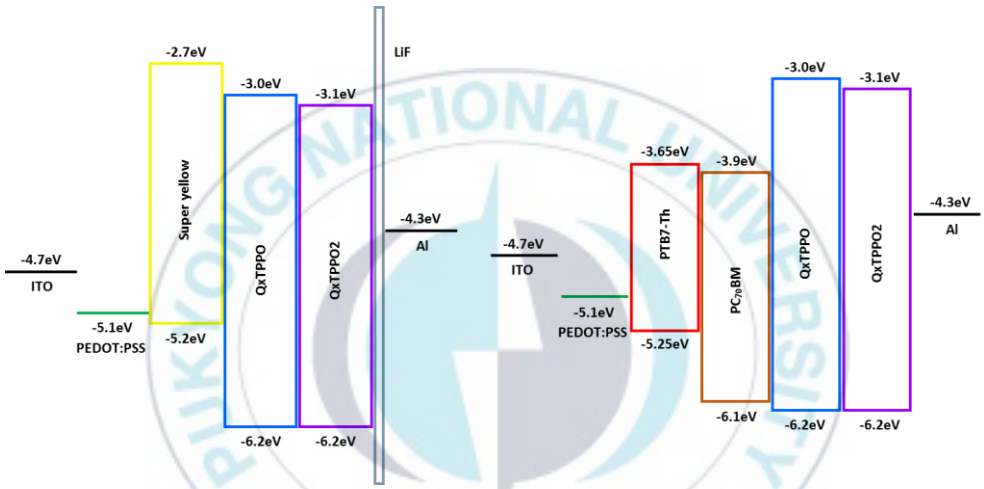

Figure III-4. Energy diagrams of OLEDs and OSCs with QxTPPO and QxTPPO2

III-2. Optoelectronic performances

Phosphine oxide-based new electron-transporting materials, QxTPPO and QxTPPO2, were explored for highly efficient OLED and OSC devices. Our new electron-transporting materials are introduced to the conventional device structure of ITO/PEDOT:PSS/Super yellow/ETL/Al (OLED device) and ITO/PEDOT:PSS/PTB7-Th:$PC_{70}BM$/ETL/Al (BHJ of OSC device) for alternating widely used ETL materials such as LiF, Ca, Ba of low WF materials with easy solution processing. The optoelectronic devices based on QxTPPO and QxTPPO2 was systematically investigated.

III-2-1. OLED device properties

To the OLED device with ETLs, these Qx ETLs were applied on top of the emissive layer, super yellow; poly(*para*-phenylenevinylene), Qx ETLs used for electron injection from Al cathode and electron transport toward emissive layer. OLED device based on Qx ETLs was systematically investigated via various concentrations. The optimal thicknesses for OLED devices are 14 nm of QxTPPO and 12 nm of QxTPPO2 at 3.0mg/ml and 2.0mg/ml respectively.

Among LiF, Qx ETLs based devices, QxTPPO-based device exhibited a maximum luminance of 19088 cd/m^2, a luminous efficiency (LE) of 15.07 cd/A, and an external quantum efficiency (EQE) of 5.31% with low turn on voltage at 2.2V. QxTPPO-based OLED device exhibited enhanced luminous efficiency compared to 12.64 cd/A of LiF-based OELD device, as well as higher EQE because of its strong dipole moment. According to energy level diagram of OLED device, the electron injection seemed to be poor, due to the energy barrier between emissive layer and Al electrode. QxTPPO is not only electron transport but also electron injection from cathode, because induced interfacial dipole lowers Al WF. As shown in Figure III-5 and Table III-2, device without ETL has much poor device properties with high turn-on voltage at 4.8V, low maximum luminance of 211 cd/m^2, luminous efficiency of 0.9 cd/A, and EQE of 0.3% because of poor electron injection. Hence, QxTPPO shows significantly important role as an ETL in OLED device.

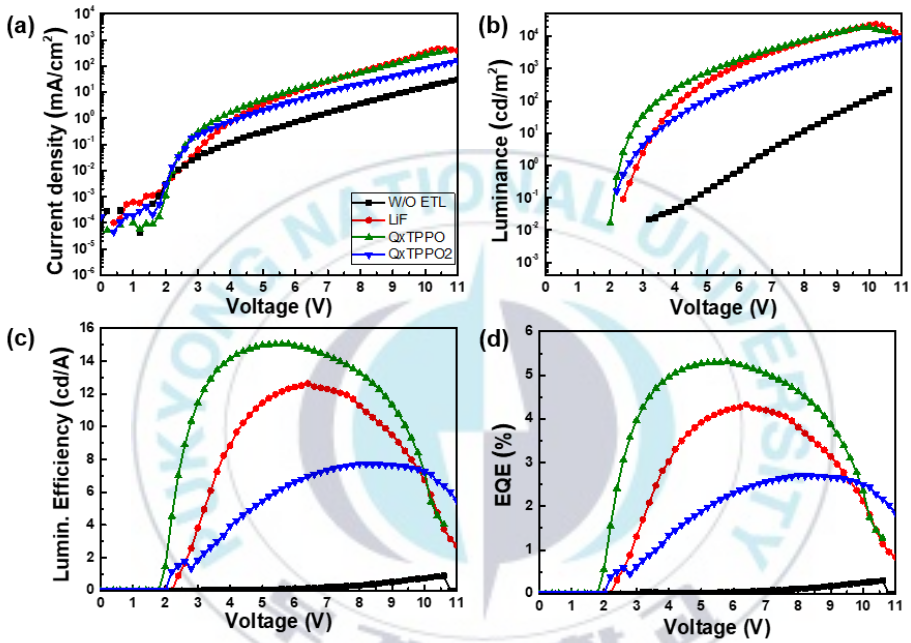

Figure III-5. OLED device characteristics with ETLs (LiF, QxTPPO, and QxTPPO2) (a) Current density vs applied voltage (J-V), (b) luminance vs the applied voltage (L-V), (c) luminous efficiency vs the applied voltage (LE-V), and (d) External quantum efficiency (EQE)

Table III-2. The optimal OLED device performances

	L_{max} [cd/m^2] @ bias	LE_{max} [cd/A] @ bias	EQE_{max} [%] @ bias	Turn-on voltage [V] @ 0.1 cd m^{-2}
W/O ETL	211 @ 10.6	0.9 @ 10.6	0.3 @ 10.6	4.8
LiF	23860 @ 10.2	12.64 @ 6.4	4.33 @ 6.4	2.6
QxTPPO	19088 @ 10.0	15.07 @ 5.8	5.31 @ 5.8	2.2
QxTPPO2	8655 @ 11.0	7.73 @ 8.0	2.71 @ 8.0	2.2

III-2-2. OSC device properties

The Qx ETLs were introduced on top of active layer, PTB7-Th of donor and $PC_{70}BM$ of acceptor, in OSC devices. These two Qx ETLs have significant improvements on photovoltaic performances. The optimized thicknesses were found to be 5 nm of QxTPPO and 6 nm for QxTPPO2. The highest power conversion efficiency (PCE) is obtained as 10.07% of QxTPPO-based device, which indicates nearly 20% enhanced photovoltaic properties compared to 8.44% without ETL device. Also 9.36% of PCE based on QxTPPO2 device is obtained (see in Figure III-6). Both Qx ETLs exhibited well-enhanced device performances, these two ETL materials have good properties as ETL in photovoltaic cells. The optimal devices based on QxTPPO exhibit significant improvements with short-circuit current density (J_{sc}) of 17.32mA/cm^2, open circuit voltage (V_{oc}) of 0.812V, a fill factor (FF) of 0.716. Compared to Al-only device, the effect of introducing QxTPPO as ETL in OSC device gives notable enhancement on all the factors such as J_{sc}, V_{oc}, and FF. The detail of photovoltaic devices is summarized in table III-3.

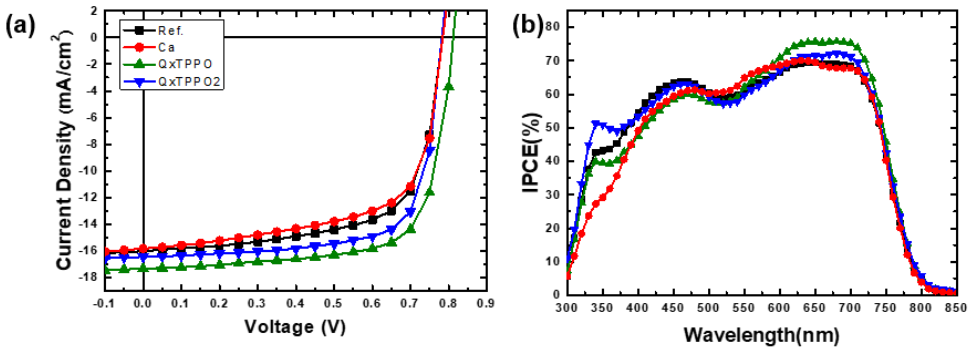

Figure III-6. OSC device characteristics with ETLs (Ca, QxTPPO, and QxTPPO2) (a) J-V curves, (b) IPCE spectra of PTB7-Th/$PC_{70}BM$-based OSCs

Table III-3. The optimal OSC device performances

	Jsc (mA/cm^2)	**Voc (V)**	**FF**	**PCE (%)**
Ref.	16.02	0.79	0.67	8.44
Ca	15.83	0.79	0.64	8.05
QxTPPO	17.32	0.81	0.72	10.07
QxTPPO2	16.45	0.79	0.72	9.36

III-2-3. Electron mobility

The electron mobility of Qx ETLs was measured by the electron-only device characteristics with space-charge limited current (SCLC) method. The electron only device of configuration is ITO/ZnO/PTB7-Th:$PC_{70}BM$/ETL/Al with and without Qx ETLs. The SCLC method equation:

$$J = \frac{9}{8}\mu_{eff}\varepsilon_0\varepsilon_r\frac{V^2}{d^3}$$

Where J is current density, μ_{eff} is the effective charge carrier mobility, ε_0 is the permittivity of free space, ε_r is the relative permittivity, d is the active layer thickness, and V is the effective voltage. The J –V characteristics of electron only devices were fitted by the Mott-Gurney law. The measured effective electron mobility (μ_{eff}) of the devices based on without, QxTPPO1, and QxTPPO2 are 2.82×10^{-4}, 4.64×10^{-4}, and 4.15×10^{-4} $cm^2\ V^{-1}\ s^{-1}$ respectively. The electron mobility of Qx ETLs-based devices is higher than that of reference device. This indicates the new electron transport materials contribute the better electron transport in the devices.

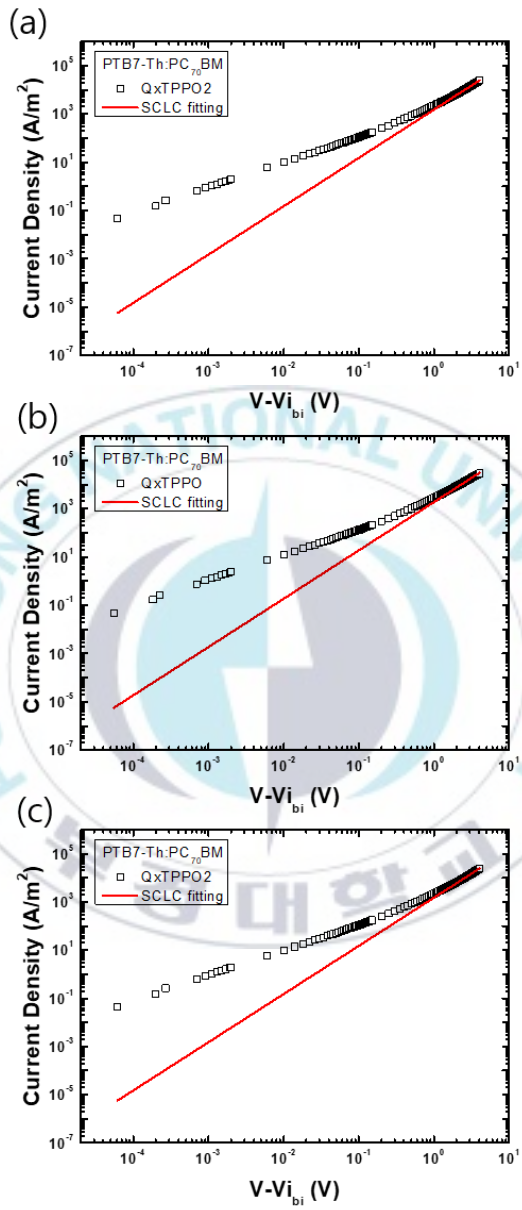

Figure III-7. J-V curves of electron-only devices characteristics (a) reference (b) QxTPPO (c) QxTPPO2 (SCLC measuerement).

III-2-4. Impedance spectroscopy

To investigate higher device efficiency, electrical impedance spectroscopy was conducted in OSC devices. The interface resistance (R_p) is significantly smaller than the reference device as shown in Figure III-8. R_p is 295, 173, and 267 Ω cm^2 of without and with QxTPPO1 and QxTPPO2 respectively. The smaller R_p indicates Qx ETLs-based devices exhibit higher device efficiency, due to efficient electron transport of Qx ETLs.

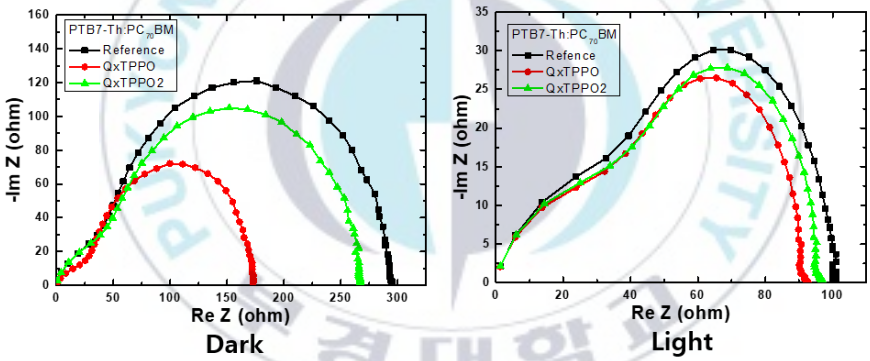

Figure III-8. Electrical impedance measurements for PTB7-Th:PC_{70}BM-based OSCs with Qx ETLs (dark and light condition).

Chapter IV. Conclusion

In conclusion, new electron transport materials consisting of quinoxaline and phosphine oxide derivatives were successfully designed and synthesized. Due to strong dipole moment of phosphine oxide, Qx ETLs are molecular structurally controlled. Qx ETLs are sufficiently soluble in alcohol solvent and able to be used solution process on the top of organic active layer. Qx ETLs exhibited transparent solution and film, non absorption in visible area confirmed through the UV-vis spectroscopy. The additional phenyl ring of QxTPPO2 contributes to conjugation length of molecule, resulting in smaller bandgap. Due to their efficient charge transport, OLEDs and OSCs have highly enhanced device performances. The optimized OLEDs show a maximum luminance of 19088 cd/m^2, a LE of 15.07 cd/A, and an EQE of 5.31% with turn-on voltage of 2.2V based on QxTPPO device which approximately 20% enhanced EQE compared to reference devices. For OSCs, optimized device with QxTPPO1 exhibited a J_{sc} of 17.32 mA/cm^2, V_{oc} of 0.81V, FF of 0.72, and PCE of 10.07%. Nearly 20% increased PCE compared to the reference devices, especially FF is significantly improved among the

factors. Thus, this interlayer study is sufficiently required for highly efficient optoelectronic devices.

References

[1] J. H. Burroughes, D. D. C. Bradley, A. R. Brown, R. N. Marks, K. Mackay, R. H. Friend, P. L. Burns, and A. B. Holmes, *Nature* 347, 539 (1990).

[2] R. H. Friend, R. W. Gymer, A. B. Holmes, J. H. Burroughes, R. N. Marks, C. Taliani, D. D. C. Bradley, D. A. Dos Santos, J. L. Bredas, M. Logdlund, and W. R. Salaneck, *Nature* 397, 121 (1995).

[3] S. Reineke, F. Lindner, G. Schwartz, N. Seidler, K. Walzer, B. Lüssem, and K. Leo, *Nature* 459, 234 (2009).

[4] G. Yu, J. Gao, J. C. Hummelen, F. Wudl, and A. J. Heeger, *Science* 270, 1789 (1995).

[5] M. Grätzel, *Nature* 367, 338 (2001).

[6] J. Y. Kim, K. Lee, N. E. Coates, D. Moses, T. Nguyen, M. Dante, and A. J. Heeger, *Science (80-.).* 222 (2007).

[7] S. H. Park, A. Roy, S. Beaupré, S. Cho, N. Coates, J. S. Moon, D. Moses, M. Leclerc, K. Lee, and A. J. Heeger, *Nat. Photonics* 3, 297 (2009).

[8] B. R. Lee, H. Choi, J. Sunpark, H. J. Lee, S. O. Kim, J. Y. Kim, and

M. H. Song, *J. Mater. Chem.* 21, 2051 (2011).

[9] B. R. Lee, J. W. Kim, D. Kang, D. W. Lee, S. J. Ko, H. J. Lee, C. L. Lee, J. Y. Kim, H. S. Shin, and M. H. Song, *ACS Nano* 6, 2984 (2012).

[10] Z. Sun, S. Shi, Q. Bao, X. Liu, and M. Fahlman, *Adv. Mater. Interfaces* 2, 1 (2015).

[11] B. R. Lee, E. D. Jung, Y. S. Nam, M. Jung, J. S. Park, S. Lee, H. Choi, S. J. Ko, N. R. Shin, Y. K. Kim, S. O. Kim, J. Y. Kim, H. J. Shin, S. Cho, and M. H. Song, *Adv. Mater.* 26, 494 (2014).

[12] Z. G. Zhang, B. Qi, Z. Jin, D. Chi, Z. Qi, Y. Li, and J. Wang, *Energy Environ. Sci.* 7, 1966 (2014).

[13] Y. Zou, H. Mao, Q. Meng, and D. Zhu, *J. Chem. Phys.* 144 (2016).

[14] D. J. Gaspar, E. Polikarpov, OLED Fundamentals, *CRC Press* (2015).

[15] Takatoshi Tsujimura, OLED Displays Fundamentals and Applications, *WILEY* (2012)

[16] A. Bemanose, M. Comte, and P. Vouaux, *J. Chim. Phys.* 50, 64 (1953).

[17] A. Bemanose, P. Vouaux, *J. Chim. Phys.* 52, 509 (1955).

[18] H. Kallmann and M. Pope, *J. Chem. Phys.* 32, 300 (1960).

[19] H. Kallmann and M. Pope, *Nature* 186(4718), 31 (1960).

[20] M. Pope, H. Kallmann, and P. Magnante, *J. Chem. Phys.* 38(8), 2042 (1963).

[21] C. W. Tang and S. A. Van Slyke, Organic electroluminescent diodes, *Appl. Phys. Lett.* 51(12), 913 (1987).

[22] J. Yuan, Y. Zhang, L. Zhou, G. Zhang, H. L. Yip, T. K. Lau, X. Lu, C. Zhu, H. Peng, P. A. Johnson, M. Leclerc, Y. Cao, J. Ulanski, Y. Li, and Y. Zou, *Joule* 3, 1140 (2019).

[23] J. Yang, H. Zhu, Y. Huang, W. Huang, and W. Wang, *RSC Adv.* 6, 100067 (2016).

[24] S. Zhang, N. E. Bauer, I. Y. Kanal, W. You, G. R. Hutchison, and T. Y. Meyer, *Macromolecules* 50, 151 (2017).

[25] D. Chen, C. Zhong, Y. Zhao, Y. Liu, and J. Qin, *Mater. Chem. Front.* 1, 2085 (2017).

[26] N. Li, S. L. Lai, W. Liu, P. Wang, J. You, C. S. Lee, and Z. Liu, *J. Mater. Chem.* 21, 12977 (2011).

[27] J. Yuan, J. Ouyang, V. Cimrová, M. Leclerc, A. Najari, and Y. Zou, *J. Mater. Chem. C* 5, 1858 (2017).

[28] Z. G. Wu, J. Zhou, L. Yu, G. Karotsis, Y. Wang, Y. X. Zheng, and Y. Pan, *J. Mater. Chem. C* 5, 8579 (2017).

[29] C. Fan, C. Duan, C. Han, B. Han, and H. Xu, *ACS Appl. Mater. Interfaces* 8, 27383 (2016).

[30] R. R. Carlson and D. W. Meek, *Inorg. Chem.* 13, 1741 (1974).

[31] A. L. Von Ruden, L. Cosimbescu, E. Polikarpov, P. K. Koech, J. S. Swensen, L. Wang, J. T. Darsell, and A. B. Padmaperuma, *Chem. Mater.* 22, 5678 (2010).

[32] W. Kan, L. Zhu, Y. Wei, D. Ma, M. Sun, Z. Wu, W. Huang, and H. Xu, *J. Mater. Chem. C* 3, 5430 (2015).

[33] B. Wang, X. Lv, B. Pan, J. Tan, J. Jin, and L. Wang, *J. Mater. Chem. C* 3, 11192 (2015).

감사의 글

대학원 과정 2 년 동안 제가 하고싶은 연구를 할수있도록 다방면으로 지지해주시고, 지도해주신 저의 지도교수님 장동욱 교수님께 진심으로 감사드립니다. 그리고 지난 2 년간 지지해주시고 도와 주신 공업화학과 문명준 교수님, 이근대 교수님, 박진환 교수님, 박성수 교수님, 진영읍 교수님, 손민영 교수님, 그리고 박치영 교수님 정말 감사합니다. 그리고 물리과 이보람 교수님 제가 소자쪽 실험도 할수있도록 환경을 제공해주시고 많은 지도해주신점 정말 감사합니다. 2 년동안의 석사과정 동안 믿고 지지해주신 부모님 그리고 친구들에게도 고마움을 표합니다. 2 년전 호주 생활을 마치고 돌아와 석사과정을 준비했었는데 벌써 2 년이라는 시간이 흘러 졸업을 하게 되었습니다. 대학원 생활동안 서로 많은 힘이 되고 도움이 되었던 친구들 문호 지현이. 문호는 앞으로 호주 그리고 박사과정 준비 잘해서 성공하자. 그리고 물리과에서 LED 소자 실험 한다고 고생하고 있을 때, 전혀 몰랐던 저를 그저 열심히 한다고 많은 도움을 준 지훈행님. 덕분에 많이 배우고, 더욱 성장할수 있는 계기가 된 것 같아요. 행님도 하시는거 준비, 마무리 잘 하시고, 하시는 일 모두 잘되시길 바래요. 그리고 우리 실험실 원들, 선배였던 민석이형, sella, 랩 mate 문호 shinta 2 년간 고생 많았고, gita, ratri, bless you, 마지막으로 실험실 후배 석우 열심히 하는 모습 정말 보기 좋지만 아직 석사 시작도 안했으니 너무 진빼지 말고, 내가 좀더 가까이서 봐주고 했으면 더 좋았을텐데 많이 도움을 못준 것 같아서 미안하네, 항상 지금처럼 열심히 하길 바란다. 석사생활동안 저를 지지해주시고 도와주신 모든 분들께 다시 한번 감사의 말씀을 드립니다.